 DOI: 10.21608/adjalexu.2023.222527.1396

CHARACTERIZATION AND TENSILE STRENGTH EVALUATION OF CHITOSAN SCAFFOLDS INCORPORATED WITH GRAPHENE OXIDE NANOPARTICLES (IN-VITRO STUDY)

Asmaa M. Ali[1*] BDS, Sonia M. Elshabrawy[2] PhD,
Elbadawy A. Kamoun[3,4] PhD

ABSTRACT

INTRODUCTION: Chitosan (CTS) has been a popular option for scaffold fabrication because of its biocompatibility, biodegradability, antimicrobial and nonimmunogenic effects. However, it is of limited function, due to its low mechanical strength and its solubility in acidified media. These limitations could be overcome by its blending with other polymers like polyvinyl alcohol (PVA) and incorporation of other bioactive material such as carbon-based nanomaterials like graphene oxide (GO) to improve its mechanical properties and tissue regeneration capability.

OBJECTIVE: Evaluation of the tensile strength of CTS-PVA-GO nanocomposites with different ratios of scaffold composition of CTS and GO

METHODS: GO nanoparticles were chemically prepared and characterized. Different concentrations of both CTS and nano-GO were used for fabrication of CTS/PVA/GO nanocomposite films through the solvent casting method. Tensile strength of the nanocomposite films was assessed after characterization by FTIR and SEM.

RESULTS: Groups were compared using Kruskal Wallis test followed by Dunn's post hoc test. There was no significant difference in tensile strength between the nanocomposite films of CTS (2%) and CTS (3%). The tensile strength decreased after addition of nano-GO at different concentrations.

CONCLUSIONS: Obtaining the best mechanical properties of CTS/PVA/GO nanocomposite scaffold for dental hard tissue engineering requires low concentrations of CTS (less than 2%) without increasing the GO concentration above 1% to prevent its aggregation.

KEYWORDS: Chitosan; Polyvinyl alcohol; Graphene oxide nanoparticles Tensile strength.

RUNNING TITLE: GO nanoparticles effect on tensile strength of chitosan scaffolds.

1-Instructor at Dental Biomaterial Department, Faculty of Dentistry, Kafr El-Sheikh University, Egypt.

2 -Professor of Dental Biomaterials, Dental biomaterials Department, Faculty of Dentistry, Alexandria University, Alexandria 21512, Egypt.

3 -Assistant Professor of Polymeric Materials Research Department, Advanced Technology and New Materials Research Institute (ATNMRI), City of Scientific Research and Technological Applications (SARTA-City), New Borg Al-Arab City, Alexandria 21934, Egypt.

4-Nanotechnology Research Center (NTRC), The British University in Egypt, Cairo, Egypt,

Corresponding author:
Asmaa.abdelrahman.dent@alexu.edu.eg

INTRODUCTION

The goal of tissue engineering is to repair damaged tissues through biologically compatible techniques. Cells, growth factors, and scaffolds are the three primary components of tissue engineering (1). Optimizing scaffolds will create the ideal conditions needed for cellular growth. For effective use, these scaffolds should meet certain criteria including biocompatibility, porosity, degradation rate, sufficient mechanical strength, sterility, and cost-effectiveness (2) Organic and synthetic polymer-based biomaterials are used for scaffold construction. Natural polymers including collagen, gelatin, chitosan, cellulose, and alginate, are biocompatible agents that can improve cellular adhesion and proliferation. However, they lack the enough mechanical strength needed for some applications, such as hard tissue engineering (3).

Synthetic polymers, Polyvinyl alcohol (PVA) as an example, are considered favorable option for tissue regeneration due to their controlled biodegradability, but they have some disadvantages, such as allowing poor migration of metabolites and causing inflammatory reactions during their degradation. In general, degradable polymers have very low mechanical properties, whereas

mechanically strong polymers are always bioinert (4).

Chitosan (CTS)-based biomaterials have widely used in various applications because of their specific criteria such as reduced foreign body reaction, antibacterial activity, biodegradability, and biocompatibility. CTS can create porous structures, which is considered a key characteristic in tissue engineering and cellular migration. It is a linear, pseudonatural, and semi-crystalline polysaccharide made up *of (1→4)-2-acetamido-2-deoxy-β-D-glucan (N-acetyl D-glucosamine) and (1→4)-2-amino-2-deoxy-β-D-glucan (D-glucosamine)* (5). Chitosan's primary amine group has a positive charge, and it is what allows chitosan to interact with negatively charged macromolecules like DNA, RNA, and other biological substances. It is also responsible for chitosan's antibacterial activity, mucoadhesiveness, and hemostatic properties (6,7). CTS, like many polysaccharides, has some inherent limitations like poor solubility and stability in physiological fluids and lack of the necessary flexibility, so it is not commonly to be used in its pure form; instead, it is combined with other materials (8).

Polyvinyl alcohol (PVA) is a water-soluble synthetic polymer with excellent biocompatibility, nontoxicity, and noncarcinogenicity, and thus, it is considered as an ideal biomaterial for use in polymer blends (9,10). It also provides an additional improvement in the flexibility of other polymers (10).

The CTS /PVA polymer blend is employed in variety of biomedical applications, such as tissue engineering (11), wound dressings (12), and drug delivery systems (13).

Carbon-based nanomaterials, including carbon nanotubes (CNTs), graphene, and graphene oxide (GO), with their exceptional mechanical, optical, electrical, and biological properties are being utilized as reinforcing agents to modify the final polymer's characteristics and performance (14).

Graphene based materials have an antimicrobial activity and can be used as an implant coating. Also, they interact with the biofilm and lead to inhibition of bacterial colonization. Antimicrobial action can be increased by functionalizing GO. Silver nanoparticles (AgNPs) may be coated on GO to create a GO/Ag nanocomposite with enhanced antibacterial properties. The nanocomposite demonstrated remarkable antibacterial action against Escherichia coli and Staphylococcus aureus (15).

GO nanosheets allow for a biocompatible platform for cellular growth and tissue regeneration (16) They have also received much interest in a different biomedical application, including drug delivery (17), bioimaging (18), tissue engineering (19) and antibacterial effects (20).

Since GO has oxygen-containing functional groups such as epoxy, carboxyl, and hydroxyl groups on its nanosheet basal plane and edge, it is more hydrophilic and easy dispersed in water than graphene and graphite powder (21,22). These functional groups offer strong interactions with polar solvents and polymer matrices, resulting in better GO dispersion (23).

Graphene oxide positively influenced the proliferation and differentiation of mesenchymal stem cells (MSCs) as reported in some in vitro cultures (24,25). It can also offer the needed properties for the development of biosensors such as good electrical conductivity, large surface area and great electromechanical activity (26). Biopolymer-GO has been introduced as GO is considered nontoxic and can improve the polymer properties even at very low concentrations compared to other reinforcing fillers (27).

This study aims to evaluate the tensile strength of CTS-PVA-GO nanocomposites with different ratios of scaffold composition of CTS and GO. The null hypothesis of the current study was that there would be no difference in the tensile strength of different concentrations of CTS and GO in the nanocomposite scaffold.

MATERIALS AND METHODS

Study design

In this *in-vitro* study, a total of 88 samples were used for characterization, evaluation of tensile strength. The sample size was calculated based on 95% confidence level and 80% study power using Rosner's method (28) calculated by *G*Power* software Version 3.0.10 (*G*Power* 2019, Universität Düsseldorf, Germany). The study samples were divided into 8 groups according to the concentration of CTS (2% - 3%) and concentration of GO (0, 0.3, 0.5 and 1%). Each group comprised 11 samples divided into 3 samples for characterization, 8 samples for evaluation of tensile strength evaluation.

Materials

Sulfuric acid (purity 95-97%) was purchased from (Riedel deHaen, Germany), hydrogen peroxide (purity ~36%) was purchased from (Pharaohs Trading, Egypt), hydrochloric acid (30%) was obtained from (El-Salam for Chemical Industries, Egypt), potassium permanganate (99%) was bought from (Longlive Co., China), graphite (200 nm mesh, 99.99% was obtained from (Alpha-Aesar, Germany), CTS powder (medium molecular weight, 75-85% deacetylated, PVA with hydrolysis degree between 98-99% and a molecular weight of 31,000–50,000 g/mol were purchased from (Sigma-Aldrich, Saint louis, MO, USA), and acetic acid were supplied by (El Goumhoria Co for chemicals, Alexandria, Egypt).

Preparation of graphene oxide nanoparticles

Graphene oxide was synthesized according to a slight modification of the Hummer method (29). Three grams of graphite powder was added to 70 ml of

concentrated H_2SO_4, and then the mixture kept stirred with a mechanical stirrer for 10 minutes while being kept in an ice bath and monitored using a thermometer to regulate its temperature rise. Over the course of one hour, 9.0 g of $KMnO_4$ was integrated gradually into the mixture and stirred at room temperature. Then, 5.0 g of potassium persulfate was gradually supplemented to the suspension. To prevent a sudden rise in reaction-temperature, an ice bath and thermometer were utilized to maintain a constant temperature of 25℃. After an hour, 15 ml of hydrogen peroxide is added after addition 500 ml of distilled water. The resultant solid underwent filtration and rinsing once with double-distilled water, once with acidic water (10% HCl), and then twice with double-distilled water. The obtained substance was dried at 70 ℃ for 48 hours in preparation for the next experiment (29).

Characterization of GO nanoparticles

Graphene oxide was characterized by different methods: Raman spectroscopy UV/Vis. Spectrophotometer-Double beam (T80+, PG instruments Ltd., UK.), Fourier transform infrared spectroscopy (FTIR analysis) (BRUKER, Germany) covering the spectrum range from 400-4000 cm^{-1}, and Scanning electron microscopy (SEM) (JEOL, JSM-5, Japan) were performed.

Preparation of chitosan–polyvinyl alcohol–graphene oxide (CTS/PVA/GO) nanocomposite films

Chitosan solution was produced in two distinct concentrations. (2 and 3 (wt./v, %) by dissolving CTS in 2% acetic acid under stirring for 5 hours at room temperature (30). Then, 10% PVA solution was created by autoclaving PVA powder with distilled water at 120°C. The polymer blend was obtained by mixing two polymeric solutions (50% CTS: 50% PVA) (31). In a solution containing 2% acetic acid, GO was dispersed at three distinct concentrations (0.3, 0.5, and 1 (wt./v, %). Sonication was utilized to ensure uniform distribution of the mixture (30,31). CTS/PVA/GO nanocomposite films were produced through a solvent-casting method. GO solution was added to the polymer blend and kept under stirring for 24 hours until a uniform mix was obtained. The solution was poured into a petri dish, and the cast film was dried in a vacuum oven at 60℃ for 24 hours (30).

Sample grouping

Samples were assigned into two main groups and one control group according to the concentration of CTS in the nanocomposite. Each main group was divided into three subgroups according to the concentration of GO nanoparticles in the nanocomposite.

Group I: Control group; (1% CTS: 1% PVA): Subgroup IA: CTS 2 (wt./v, %) and subgroup IB: CTS 3 (wt./v, %).

Group II: (1% CTS: 1% PVA): CTS 2 (wt./v, %): Subgroup IIA: GO 0.3 (wt./v, %), subgroup IIB: GO 0.5 (wt./v, %) and subgroup IIC: GO 1 (wt./v, %).

Group III: (1% CTS: 1% PVA): CTS 3 (wt./v, %): Subgroup IIIA: GO 0.3 (wt./v, %), subgroup IIIB: GO 0.5 (wt./v, %) subgroup IIIC: GO 1 (wt./v, %).

Instrumental characterization of prepared CTS/PVA/GO nanocomposite films

The nanocomposite was characterized by FTIR analysis to obtain information about the functional groups associated with the prepared nanocomposite and by SEM. Evaluation of tensile strength of the nanocomposite was conducted according to (ISO 2062:2009) specifications. The extension rate was maintained at 5 mm/min and the employed cell load was 20 N with a gauge length of 30 mm (30). The dimensions of the samples were (6 cm × 1 cm) (32). The tensile strength was evaluated for both CTS/PVA and CTS/PVA/GO nanocomposite films nanocomposite films to assess the effect of GO incorporation on the scaffold by universal testing machine (.Thermo scientific ELED 3625A, USA).

Statistical analysis

All variables were presented mainly using median, interquartile range (IQR), minimum and maximum values in addition to mean and standard deviation (SD). Variables were compared using Kruskal Wallis test followed by Dunn's post hoc test with Bonferroni correction. The significance level was set at a p value of 0.05. Data were analyzed using IBM SPSS (Version 23.0).

RESULTS

Characterization of GO nanosheets

Raman spectroscopy

In Raman spectra of the structure of GO as illustrated in (Fig. 1), The G band was found to be broad, and shifted to ν 1605 cm^{-1}, while the D band was found to have high intensity, due to disordering in the sp^2 structure. The D band was observed at ν 1354 cm^{-1}.

Fourier transform infrared spectroscopy analysis

Spectrum of GO is illustrated in (Fig. 2a), which exhibits multiple peaks related to multiple functional groups containing oxygen that confirm the formation of GO nanosheets. Bands at approximately ν 1709 cm^{-1}, 1091-1042 cm^{-1} and 3243 cm^{-1} are related to C=O (carboxyl or carbonyl), C-O (epoxy or alkoxy) and O-H stretching of the COOH group; respectively. Peak at approximately 811 cm^{-1} is attributed to aromatic C-H deformation. Spikes at ν 646, 575 and 495 cm^{-1} arise from C-H bending vibration. The band at ν 1627 cm^{-1} is related to remaining sp^2 structure.

Scanning electron microscopy investigation

From (Fig. 3a), it is observed that the synthesized GO has a layered structure which is related to ultrathin homogenous films that may be folded or continuous. Sheets' edges can be observed with kinked or wrinkled areas. Sometimes

GO particles are closely attached to each other and form aggregates.

Characterization of the prepared CTS/PVA/GO nanocomposite films

Macroscopic investigation of CTS/ PVA/GO nanocomposite films

In general, CTS/PVA films are yellowish in color with some translucency due to the PVA. Addition of GO made the films turn black and the intensity of the black color increased by increasing GO amount. When the thickness of the films was measured by a digital caliber, it is found to be 0.2 mm.

Fourier transform infrared spectroscopy analysis

Fourier transform infrared spectroscopy spectra of PVA, CTS, CTS/PVA and CTS/PVA/GO with different ratios (0.3, 0.5, and 1%) are illustrated in (Fig. 2). The PVA infrared spectrum (Fig. 2b) displayed a distinctive diffraction peak at 3279 cm^{-1} which refers to intermolecular hydrogen bonding and -OH stretching vibrations. The vibrational spectrum detected at ν 2908 cm^{-1} is related to C-H stretching from the alkyl group. Another peak is observed at ν 1086 cm^{-1} which is related to C-O stretching. The CTS spectrum (Fig. 2c) displayed a wide broad band at 3360 cm^{-1} because of the overlapping of -OH and -NH stretching vibrations. The peak at 2868 cm^{-1} corresponds to the vibrational stretching of CH_2. Another band at 1590 corresponds to -NH bending (NH_2). The carbonyl stretching from C-H bending and C-O-C linking are shown by the bands at ν 1376 and 1150 cm^{-1}. In the CTS/PVA polymer blend (Fig 2d), the intensity of the ν 3279 cm^{-1} peak decreased to ν 3268 cm^{-1}. Additionally, a rise in the absorption band's intensity matching to the C-H stretching vibration was detected at ν 2938 cm^{-1}. The peak at ν 1327 cm^{-1} also confirmed the crosslinked structure with PVA because of the deformation vibration of CH_2. The peak at ν 1651 cm^{-1} corresponds to C=N stretching due to the reaction of chitosan's amino groups and hydroxyl groups related to PVA.

In the CTS/PVA/GO nanocomposite (Fig 2e), the strong characteristic peak at ν 3268 cm^{-1} is corresponding to the -OH group present in GO and the stretching of the NH_2 group in CTS. The peaks at ν 1410 and 1143 cm^{-1} are related to carboxylate vibrations. The vibrational peak at ν 1643 cm^{-1} is related to the vibrational deformation of absorbed water molecules. Another characteristic peak at ν 1554 cm^{-1} is related to the amino groups of CTS. The peak at ν 2907 cm^{-1} is related to the C-H stretching vibration. The bands at ν 923 and 847 cm^{-1} are related to the polysaccharide structure present in CTS.

Scanning electron microscopy investigation

The microstructures of the polymer blend (CTS and PVA) and nanocomposite films were assessed by SEM. Images are presented in (Fig. 3). The polymer blend (Fig 3b,3c) shows a smooth surface which indicates a uniform dispersion and good miscibility between the two polymers. The surfaces of the pure CTS and pure PVA films are relatively very smooth, so the blend between them is expected to be of the same condition. The morphology of the nanocomposite of 1CTS (2%):1PVA with GO (0.3,0.5,1%) respectively (Figs. 3d, 3e and 3f) showed a rough surface which is related to the GO dispersion. As the ratio of GO increases, it completely covers the polymer surface, making it rougher and less noticeable. This is attributed to GO and the polymer's strong interaction. The morphology of the nanocomposite of 1CTS (3%):1PVA with GO (0.3,0.5,1%) respectively is showed in Figs. 3g, 3h and 3i). Aggregation of GO particles is obvious especially at higher concentration.

Mechanical properties evaluation

Tensile strength evaluation

There was no significant difference in tensile strength between 1CTS (2%):1 PVA and 1CTS (3%):1PVA. The addition of GO decreased the tensile strength for different concentrations (0.3, 0.5 and 1%) as shown in Table (1).

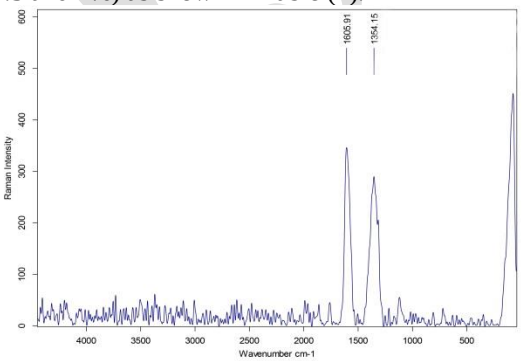

Figure (1) Raman spectroscopy of graphene oxide nanoparticles.

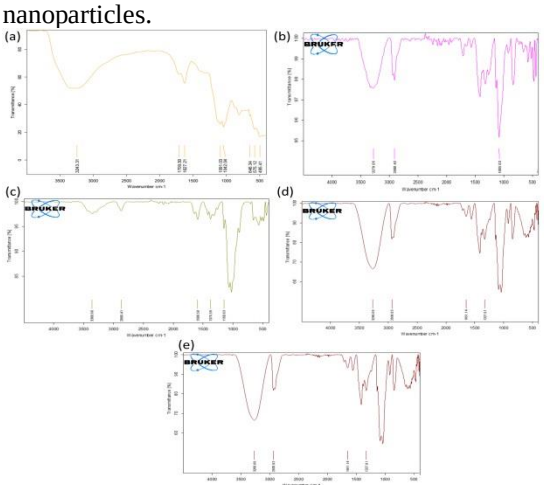

Figure (2) FTIR spectra of (a) GO, (b) PVA, (c) CTS, (d) CTS/PVA blend, and (e) CTS/PVA/GO.

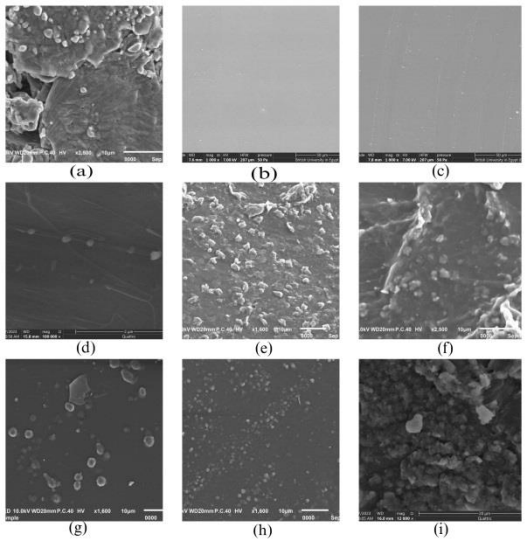

Figure (3) SEM micrographs of (a) GO nanosheets, (b) 1CTS (2%):1PVA polymer blend, (c) 1CTS (3%):1PVA polymer blend, (d) 1CTS (2%):1PVA with 0.3% GO, (e)1CTS (2%):1PVA with 0.5% GO. (f) 1CTS (2%):1PVA with 1% GO. (g) 1CTS (3%):1PVA with 0.3% GO, (h) 1CTS (3%):1PVA with 0.5% GO.
(i) 1CTS (3%):1PVA with 1% GO.

Table 1: Tensile strength results of the studied groups of CTS-PVA-GO nanocomposite films.

	1CTS (2%): 1PVA	1CTS (2%): 1PVA + 0.3 %GO	1CTS (2%):1PVA +0.5 %GO	1CTS (2%): 1PVA +1 %GO	1CTS (3%): 1PVA	1CTS (3%): 1PVA+0.3% GO	1CTS (3%):1PVA +0.5%GO	1CTS (3%): 1PVA+ 1% GO
Mean (SD)	8.49 (1.25)	4.17 (0.34)	4.04 (0.83)	6.27 (0.50)	10.00 (0.55)	6.00 (0.56)	8.42 (0.64)	3.77 (0.56)
Median	9.40	4.11	4.46	6.10	10.25	6.10	8.50	3.47
Min – Max (MPa)	6.45 – 9.50	3.54 – 4.50	2.84 – 5.05	5.75 – 7.30	9.40 – 10.70	5.05 – 6.75	7.55 – 9.05	3.06 – 4.42
P value	**<0.0001***							

*Statistically significant difference at p value ≤ 0.05

DISCUSSION

The production of GO is affected by multiple variables, such as the acid concentration, strength of the oxidizing agent and the breakdown of the formed intermediate compound. The addition of strong sulfuric acid to graphite leads to its intercalation, and graphite bisulfate is formed (graphite intercalated compound). After expanding the graphene layer, another intercalation occurs at the basal plane. Amorphization occurs gradually and the interlayer distance increases. Additionally, the lattice parameter along the c-axis (axis perpendicular to the carbon layers) decreases and the number of layers decreases. By addition of $KMNO_4$, there is ultrasonic cleavage of graphite oxide with a significant number of hydroxyl, carboxyl, and epoxy groups on its surface. These oxygen functional groups will increase the distance between layers and make the structure more hydrophilic (33,34).

Raman spectroscopy is used to study the disorder and defects in the crystal structure of carbonaceous materials. This indicates the presence of the G band that arises from stretching of the C-C bond and as graphite disordering increases, this G band becomes broad at ν1605 cm^{-1}, and a broader D band is observed at ν1354 cm^{-1}. According to Yuan et al. (2017), the presence of broad and intense G and D bands is related to higher degrees of oxidation in comparison to other samples with lower oxidation degrees (35). Additionally, the I_D / I_G ratio describes sp^2 / sp^3 carbon ratio, which is corresponding to the defects created by the attachment of the functional groups to carbon, as this is indicative of the aromatic structure's integrity. If this ratio reaches 0.8, this indicates structural defects produced by oxidation and attachment of the functional groups (36).

Fourier transform infrared spectroscopy characterization of GO reveals oxygen atoms existence in the form of -OH, C=O, and C-O, which confirmed the oxidation process and GO formation. These hydrophilic functional groups are very important in the compatibility between GO and the polymeric matrix. Additionally, these abundant functional groups could improve GO hydrophilicity (32). As the number of these functional groups increases, there is more attraction between them and other particles like silver nanoparticles (AgNPs). This has been confirmed when GO/AgNP nanocomposite has been investigated as an implant coat for NiTi alloy(37).

For preparation of the nanocomposite, CTS was added to PVA and then different concentrations (0.3, 0.5, and 1%) of GO were added to the polymer blend. FTIR analysis of pure PVA presented a spectrum related to its hydroxyl groups. The combination of frequencies produced by the stretching vibrations of the backbone aliphatic CH, CH-OH, and CO. The CTS spectrum shows bands related to N-H and C-H stretching. For the CTS/PVA polymer blend, increasing the intensity of C-H stretching indicated good miscibility between PVA and CTS. The decrease in intensity of the band of -OH stretching in the polymer blend, compared to pure PVA which might be due to the vibrational stretching of –OH of PVA with

secondary –NH groups related to CTS through intermolecular hydrogen bonding. By the addition of GO, the nanocomposite indicated its presence within the blend through the formation of a hydrogen bond between GO and the polymer blend. The band at ν 3268 cm^{-1} appears to be increased to ν 3271 cm^{-1} due to the stretching vibration of hydroxyl groups related to GO (38).

The tensile strength of the films decreases as the CTS concentration increases. This might be because of the excessive CTS which prevents the GO sheets from assembling into high-orientation structures, and this resulted in a significant number of nanoscale defects that limited the performance of the materials. In a previous study, a CTS concentration of 0.3% showed an improvement in the tensile strength after the addition of GO, but when the CTS concentration increased to 0.5% and 1%, the tensile strength decreased (39). Since the electrostatic interaction is thought to be more powerful than hydrogen bonding, it can be considered the main driving force. Due to the high electrostatic attraction between CTS and GO, addition of excess CTS prevents the formation of a randomly and sparsely distributed structure and can lead to precipitation of GO (40).

CONCLUSIONS

High concentrations of CTS that were used in this study lead to aggregation of GO nanoparticles rather than their dispersion and orientation. As a result, no improvement in tensile strength was noted. The formulation used in this study can be used as a wound dressing to get the benefits of antimicrobial action of CTS and GO. Obtaining the best mechanical properties for dental hard tissue engineering requires low concentrations of CTS (less than 2%) without increasing the GO concentration above 1% to prevent its aggregation.

Limitations

Lacking biocompatibility testing and investigation of antibacterial action of the prepared scaffold.

RECOMMENDATIONS

Biocompatibility and cell viability tests are recommended for the prepared scaffolds.

In-vivo testing for the scaffold with different GO concentrations to detect if there is a critical concentration that cause any adverse reactions

Scaffold may be loaded with antimicrobial drug to enhance antimicrobial action and investigate the release properties of the scaffold.

CONFLICT OF INTEREST

Authors declare that they have no competing interests.

FUNDING STATEMENT

This research did not receive any specific grant from funding agencies in public, commercial, or not for profit sectors.

Acknowledgments

Authors would like to thank Dr. Hams Hamed for her help in statistical analysis.

REFERENCES

1. O'brien FJ. Biomaterials & scaffolds for tissue engineering. Mater Today. 2011;14:88–95.
2. Bose S, Roy M, Bandyopadhyay A. Recent advances in bone tissue engineering scaffolds. Trends Biotechnol. 2012;30:546-54.
3. Dhandayuthapani B, Yoshida Y, Maekawa T, Kumar DS. Polymeric scaffolds in tissue engineering application: a review. Int J Polym Sci. 2011;2011:1-19.
4. Surudžić R, Janković A, Bibić N, Vukašinović-Sekulić M, Perić-Grujić A, Mišković-Stanković V, et al. Physico–chemical and mechanical properties and antibacterial activity of silver/poly (vinyl alcohol)/graphene nanocomposites obtained by electrochemical method. Compos B Eng. 2016;85:102–12.
5. Muxika A, Etxabide A, Uranga J, Guerrero P, de La Caba K. Chitosan as a bioactive polymer: Processing, properties and applications. Int J Biol Macromol. 2017;105:1358–68.
6. Ke CL, Deng FS, Chuang CY, Lin CH. Antimicrobial actions and applications of chitosan. Polymers (Basel). 2021;13:904.
7. Kim IY, Seo SJ, Moon HS, Yoo MK, Park IY, Kim BC, et al. Chitosan and its derivatives for tissue engineering applications. Biotechnol Adv. 2008;26:1–21.
8. Chen S, Wang H, Jian Z, Fei G, Qian W, Luo G, et al. Novel poly (vinyl alcohol)/chitosan/modified graphene oxide biocomposite for wound dressing application. Macromol Biosci. 2020;20:1900385.
9. Kamoun EA, Kenawy ERS, Chen X. A review on polymeric hydrogel membranes for wound dressing applications: PVA-based hydrogel dressings. J Adv Res. 2017;8:217–33.
10. Chetouani A, Elkolli M, Bounekhel M, Benachour D. Chitosan/oxidized pectin/PVA blend film: Mechanical and biological properties. Polymer Bulletin. 2017;74:4297–310.
11. Agrawal P, Pramanik K. Chitosan-poly (vinyl alcohol) nanofibers by free surface electrospinning for tissue engineering applications. Tissue Eng Regen Med. 2016;13:485–97.
12. Farzinfar E, Paydayesh A. Investigation of polyvinyl alcohol nanocomposite hydrogels containing chitosan nanoparticles as wound dressing. Int J Polym Mater. 2019;68:628–38.
13. Cui Z, Zheng Z, Lin L, Si J, Wang Q, Peng X, et al. Electrospinning and crosslinking of polyvinyl alcohol/chitosan composite nanofiber for transdermal drug delivery. Adv. Polym. Technol. 2018;37:1917–28.
14. Ge C, Lao F, Li W, Li Y, Chen C, Qiu Y, et al. Quantitative analysis of metal impurities in carbon nanotubes: efficacy of different pretreatment protocols for ICPMS spectroscopy. Anal Chem. 2008;80:9426–34.
15. V Srimaneepong, HE Skallevold, Z Khurshid, MS Zafar, D Rokaya, J Sapkota Graphene for

antimicrobial and coating application. Int J. mol. Sci. 2022;23:499–516.
16. Yu P, Bao RY, Shi XJ, Yang W, Yang MB. Self-assembled high-strength hydroxyapatite/graphene oxide/chitosan composite hydrogel for bone tissue engineering. Carbohydr Polym. 2017;155:507–15.
17. Xiong S, Luo J, Wang Q, Li Z, Li J, Liu Q, et al. Targeted graphene oxide for drug delivery as a therapeutic nanoplatform against Parkinson's disease. Biomater Sci. 2021;9:1705–15.
18. Lee SY, Kwon M, Raja IS, Molkenova A, Han DW, Kim KS. Graphene-Based Nanomaterials for Biomedical Imaging. In: Han D, Hong SW, (eds). Multifaceted Biomedical Applications of Graphene, Germany: Springer; 2022, pp 125–48.
19. Zhihui K, Min D. Application of graphene oxide-based hydrogels in bone tissue engineering. ACS Biomater Sci Eng. 2022;8:2849–57.
20. Wei P, Wang L, Xie F, Cai J. Strong and tough cellulose–graphene oxide composite hydrogels by multi-modulus components strategy as photothermal antibacterial platform. J Chem Eng. 2022;431:133964.
21. Mazaheri M, Akhavan O, Simchi A. Flexible bactericidal graphene oxide–chitosan layers for stem cell proliferation. Appl Surf Sci. 2014;301:456–62.
22. Sohail M, Saleem M, Ullah S, Saeed N, Afridi A, Khan M, et al. Modified and improved Hummer's synthesis of graphene oxide for capacitors applications. Mod Electron Mater. 2017;3:110–6.
23. Venkataprasanna KS, Prakash J, Vignesh S, Bharath G, Venkatesan M, Banat F, et al. Fabrication of Chitosan/PVA/GO/CuO patch for potential wound healing application. Int J Biol Macromol. 2020;143:744–62.
24. Unnithan AR, Park CH, Kim CS. Nanoengineered bioactive 3D composite scaffold: A unique combination of graphene oxide and nanotopography for tissue engineering applications. Compos B Eng. 2016;90:503–11.
25. Cao L, Zhang F, Wang Q, Wu X. Fabrication of chitosan/graphene oxide polymer nanofiber and its biocompatibility for cartilage tissue engineering. Mater Sci Eng C. 2017;79:697–701.
26. Krishnan SK, Singh E, Singh P, Meyyappan M, Nalwa HS. A review on graphene-based nanocomposites for electrochemical and fluorescent biosensors. RSC Adv. 2019;9:8778–881.
27. Yenier Z, Seki Y, Şen İ, Sever K, Mermer Ö, Sarikanat M. Manufacturing and mechanical, thermal and electrical characterization of graphene loaded chitosan composites. Compos B Eng. 2016;98:281–7.
28. Rosner B. Fundamentals of biostatistics. 8th ed. Canada: Nelson Education; 2015.
29. Abd-Elhamid AI, Kamoun EA, El-Shanshory AA, Soliman HMA, Aly HF. Evaluation of graphene oxide-activated carbon as effective composite adsorbent toward the removal of cationic dyes: Composite preparation, characterization, and adsorption parameters. J Mol Liq. 2019;279:530–9.
30. Tavakoli M, Karbasi S, Bakhtiari SSE. Evaluation of physical, mechanical, and biodegradation of chitosan/graphene oxide composite as bone substitutes. Polym-Plast Tech Mat. 2019;59:1–11.
31. Pandele AM, Ionita M, Crica L, Vasile E, Iovu H. Novel Chitosan-poly (vinyl alcohol)/graphene oxide biocomposites 3D porous scaffolds. Compos B Eng. 2017;126:81–7.
32. Yadav M, Ahmad S. Montmorillonite/graphene oxide/chitosan composite: Synthesis, characterization and properties. Int J Biol Macromol. 2015;79:923–33.
33. Aliyev E, Filiz V, Khan MM, Lee YJ, Abetz C, Abetz V. Structural characterization of graphene oxide: Surface functional groups and fractionated oxidative debris. Nanomaterials. 2019;9:1180.
34. Bîru EI, Iovu H. Graphene nanocomposites studied by Raman spectroscopy. In: do Nascimento GM, editor. Raman Spectroscopy, London, UK: Intechopen; 2018. P. 179.
35. Yuan R, Yuan J, Wu Y, Chen L, Zhou H, Chen J. Efficient synthesis of graphene oxide and the mechanisms of oxidation and exfoliation. Appl Surf Sci. 2017;416:868–77.
36. Abd-Elhamid AI, Aly HF, Soliman HAM, El-Shanshory AA. Graphene oxide: Follow the oxidation mechanism and its application in water treatment. J Mol Liq. 2018;265:226–37.
37. D Rokaya, V Srimaneepong, J Qin, K Siraleartmukul, V Siriwongrungson. Graphene Oxide/Silver Nanoparticle Coating Produced by Electrophoretic Deposition Improved the Mechanical and Tribological Properties of NiTi Alloy for Biomedical Applications. J. Nanosci. Nanotechnol. 2019;23: 3804-10.
38. Das L, Das P, Bhowal A, Bhattachariee C. Synthesis of hybrid hydrogel nano-polymer composite using Graphene oxide, Chitosan and PVA and its application in waste water treatment. Environ Technol Innov. 2020;18:100664.
39. Geng L, Lin Y, Chen S, Shi S, Cai Y, Li L, et al. Superior strength and toughness of graphene/chitosan fibers reinforced by interfacial complexation. Compos Sci Technol. 2020;194:108174.
40. Qi C, Zhao L, Lin Y, Wu D. Graphene oxide/chitosan sponge as a novel filtering material for the removal of dye from water. J Colloid Interface Sci. 2018;517:18–27.